



Photolithographically patterned silver nanowire electrodeposition

S.C. Kung, W. Xing, K.C. Donovan, F. Yang, R.M. Penner*

Department of Chemistry, University of California, Irvine, CA 92697-2025, USA

ARTICLE INFO

Article history:

Received 17 December 2009
Received in revised form 18 February 2010
Accepted 21 February 2010
Available online 6 March 2010

Keywords:

Silver
Nanowire
Metal
Electrodeposition
Polycrystalline
Photolithography

ABSTRACT

We report the fabrication of silver nanowires using lithographically patterned nanowire electrodeposition (LPNE). The LPNE synthesis of silver nanowires proceeds by lithographically patterning, and then etching an evaporated nickel film to produce a nickel nanoband 20–80 nm in height. This nanoband, which traces the perimeter of the exposed region, is recessed by ≈ 500 nm into the photoresist producing a horizontal trench. A silver nanowire, of controlled height and width, is formed within this trench by electrodepositing silver from either of two aqueous solutions at the nickel nanoband. Silver nanowires with controlled widths ranging from 100 to 400 nm were obtained and the height of silver nanowires was independently controllable over the range from 20 to 80 nm. The LPNE process is wafer-scale and continuous silver nanowires millimeters in length are readily obtained. Data for the characterization of these nanowires using AFM, TEM, and XRD is presented.

© 2010 Elsevier Ltd. All rights reserved.

1. Introduction

Among the noble metals, silver occupies a position of prominence because of its plasmonic properties [1–9]. The exploitation of these properties has motivated efforts to create silver nanostructures using wet chemical methods [10], hydrothermal methods [11], vapor–liquid–solid (VLS) growth [7], metal amplification [12], and electrodeposition within porous templates [13–16]. Earlier, we developed methods for preparing ensembles of silver nanowires by electrochemical step edge decoration (ESED) [17–20], but the minimum diameter of these nanowires was in the 100 nm range. Moreover, ESED does not enable the control of nanowire position, orientation or number density – a serious liability.

Recently, we have developed a new method for the wafer-scale patterning of metal and semiconductor nanowires on dielectrics [21–25]. The purpose of this paper is to describe the adaptation of this method, called lithographically patterned nanowire electrodeposition (LPNE), to the growth of silver nanowires. Previously, LPNE has been used to prepare metal nanowires composed of platinum [21,23,25], palladium [21,23–25], gold [21,23,25–27], and bismuth [21]. The application of the LPNE method to the growth of silver nanowires presents a new challenge as compared with these other metals: the facile electron transfer kinetics of silver promotes a rapid, diffusion-controlled growth and a propensity towards dendritic deposition. In this paper, we describe methods for over-

coming this issue for two types of plating solutions – a sulfate-based plating solution containing saccharine and a commercial, cyanide-free plating solution for silver (Clean Earth Solutions™, 45.220).

2. Experimental methods

2.1. Nanowire fabrication

The seven-step LPNE procedure was used exactly as previously described [21,23,25] to produce the silver nanowires described here (Fig. 1) – except for the fifth step of the process involving silver electrodeposition. The evaporated nickel film, which functions as the working electrode for nanowire growth, has a (1 1 1) domain orientation and a grain diameter of ≈ 15 nm, based on XRD analysis. Silver nanowires were electrodeposited in the lithographically produced trench using a one-compartment three-electrode electrochemical cell controlled by a Gamry G300 potentiostat in conjunction with a computer. During this deposition, the nickel nanoband electrode functions as the working electrode. The entire lithographically patterned region was immersed in an aqueous plating solution with the exception of one edge where an electrical contact to the nickel layer was established with an alligator clip. A saturated mercurous sulfate electrode (MSE) and a 1 cm² platinum foil were used as the reference and the counter electrode, respectively. All potentials were given with respect to this reference electrode. Either of two unstirred plating solutions were used for silver deposition: *solution 1* – Aqueous (Millipore Milli-Q, $\rho > 18$ M Ω cm), 1 mM silver sulfate (Aldrich, 99.999%), 1 mM saccharine (Aldrich, 98+%), and 100 mM sodium sulfate (FisherBiotech, 99.0%) at pH 1.7 obtained by the addition of sulfuric acid (J. T. Baker, ULTREX ultra-pure); *solution 2* – a commercial silver plating solution (Clean Earth

* Corresponding author at: Department of Chemistry, University of California, 1102 Natural Sciences II, Irvine, CA 92697-2025, USA. Tel.: +1 949 824 8572; fax: +1 949 824 8125.

E-mail address: rmpenner@uci.edu (R.M. Penner).

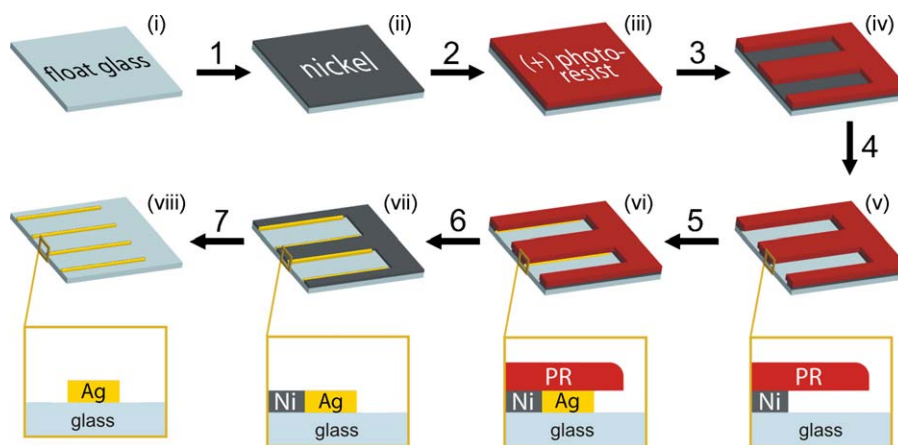


Fig. 1. Schematic diagram of the lithographically patterned nanowire electrodeposition (LPNE) process, which involves seven-step fabrication process.

Solutions™, 45.220). The procedures for silver nanowire electrodeposition were optimized for these two plating solutions as follows: for solution 1, a nucleation pulse of -0.3 V vs. MSE for 10 ms was applied followed by potentiostatic growth at -0.070 V vs. MSE for 50–400 s, depending on the desired width. For solution 2, a 750 ms nucleation pulse of -1.4 V vs. MSE was applied followed by potentiostatic growth at -0.475 V vs. MSE for ranging from 50 to 500 s.

2.2. Microscopy

Optical micrographs were acquired using a Carl Zeiss Axioskop2 equipped with bright field objectives. Scanning electron microscopy (SEM) images were obtained using a Philips XL-30 FEGSEM (field emission gun scanning electron microscope) equipped with the elemental analysis capability of energy-dispersive X-ray spectroscopy (EDX), operated at 10 keV. All samples were sputter coated with Au/Pd alloy prior to imaging to eliminate charging. Transmission electron microscopy (TEM) images and selective area electron diffraction (SAED) were acquired on a Philips CM 20 TEM at a 200 keV accelerating voltage. In order to prepare TEM specimens, silver nanowires were produced on a photoresist (PR) pre-coated surface that facilitate the release of these nanowires by dissolution of the photoresist. PR-supported silver nanowires were transferred onto a carbon film coated Cu grid (Ted Pella, Inc.) using an acetone stream (which dissolved the PR layer). Transferred nanowires were dried overnight before imaging. Noncontact mode atomic force microscopy (AFM) analysis was conducted using a MFP-3D™ stand alone atomic force microscope (Asylum Research) with Olympus, AC160TS tips in a laboratory air ambient.

2.3. X-ray diffraction

Grazing incidence X-ray diffraction (GIXRD) was performed on arrays of thousands of silver nanowires patterned on glass at 2–5 μm pitch, using a Rigaku Ultima III X-ray diffractometer employing parallel beam optics with an incident angle of 0.3° . The Cu $K\alpha$ irradiation was operated at 40 kV and 44 mA. The specimens were scanned from $2\theta = 15^\circ$ to 85° with step-scan increments of 0.1° and a dwell time at each increment of 20 s.

3. Results and discussion

3.1. Silver nanowire deposition

LPNE (Fig. 1) has been used previously to deposit nanowires composed of platinum [21,23,25], palladium [21,23–25], gold [21,23,25–27], and bismuth [23]. Nickel was used as the “sacrificial”

electrode for all of these metals except bismuth where silver was substituted. Nickel is used in this application because it is capable of functioning as an efficient working electrode and it can be selectively removed at the end of the deposition process using nitric acid (Fig. 1, step 7) which does not dissolve noble metals. For bismuth nanowires, the silver sacrificial electrode is removed using a peroxide/ammonia etch. Nickel, however, is fully compatible with silver nanowire growth.

The silver nanowire electrodeposition process is examined next. We explored the properties of two plating solutions for silver nanowire growth: *solution 1* – a sulfate-based solution containing saccharine, and *solution 2* – a commercial, cyanide-free plating solution (Clean Earth Solutions™, 45.220). Two different electrodes were employed in these cyclic voltammetric investigations: evaporated nickel films on glass (area ≈ 3 cm², Fig. 2a and d) and LPNE patterned nickel nanoband electrodes (Fig. 2b and e). One important difference between the two plating solutions can be seen by comparing the stripping potential for silver in Fig. 2a and b (*solution 1*) and that seen in Fig. 2d and e (*solution 2*). This potential – which approximates $E_{\text{Ag}^+/\text{Ag}}^0$ in these solutions – is shifted in the negative direction by approximately 0.40 V for *solution 2*. This shift reveals the presence of complexing agents for Ag^+ in this commercial plating solution; in *solution 1*, silver is uncomplexed. Other differences in the kinetics of silver deposition at these two electrodes from these two plating solutions are also apparent. In *solution 1*, silver electrodeposition proceeds on a clean evaporated nickel surface at $-(0.10\text{--}0.15)$ V (Fig. 2a, scan 1). A somewhat more negative onset for silver deposition is seen for the CVs recorded at the patterned nickel nanoband, with deposition onsets in the range from $-(0.20\text{--}0.25)$ V (Fig. 2b, scan 1). For both electrodes, a more positive onset for silver deposition is seen on scans 2 and 3. This positive shift is attributed to the presence on the nickel surface of residual silver that facilitates the renucleation and growth of silver on these subsequent scans. Thus, the observation of this shifted silver deposition onset implies that silver is incompletely removed from the nickel surface by anodic stripping in *solution 1*.

Of course in *solution 2* the onset for silver deposition is shifted negatively as compared with *solution 1* because of the -0.40 V shift in E^0 . However beyond this thermodynamic shift, the overpotential for silver deposition (referenced to E^0) is larger than the overpotentials observed in *solution 1* at both types of electrodes indicating that silver nucleation is impeded in *solution 2*. For example, at the flat nickel electrode no significant plating current is seen on the first scan until -0.80 V (Fig. 2d) – an overpotential of ~ -0.40 V – which compares with an overpotential in *solution 1* of just ~ -0.10 V (Fig. 2a). The onset for silver deposition on subse-

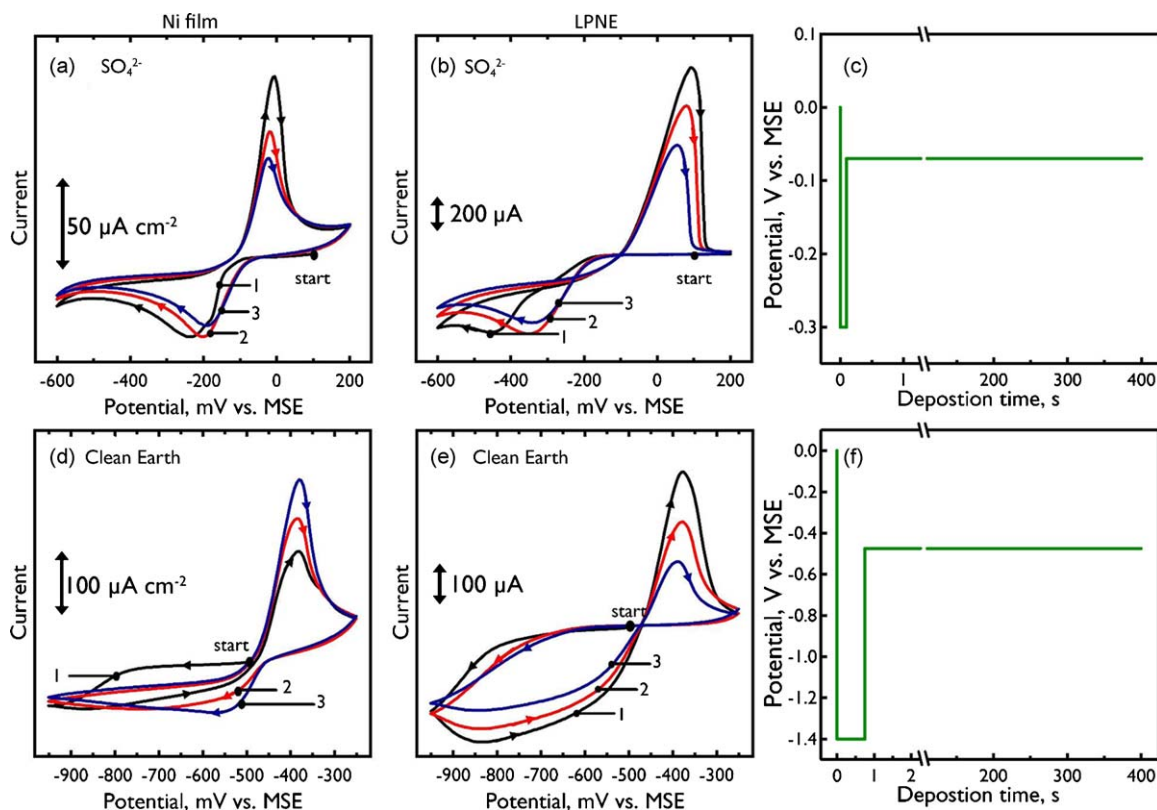


Fig. 2. Cyclic voltammograms (50 mV/s) (a) for the nickel film and (b) for the nickel nanoband in solution 1, and (d) for the nickel film and (e) for the nickel nanoband in solution 2. Pulse waveforms employed to produce silver nanowires from (c) solution 1 and (f) solution 2. Solution 1 – the sulfate-based aqueous bath containing 1 mM silver sulfate, 1 mM saccharine, and 100 mM sodium sulfate at pH 1.7; Solution 2 – Clean Earth Solutions™, 45.220.

quent scans is shift positively by more than 0.30 V, again suggesting that silver is not quantitatively removed from the nickel surface on the positive-going voltammetric scan. In solution 2, a diffusional wave for silver deposition – a prominent feature of the deposition in solution 1 – is hardly observed on these subsequent scans suggesting that the rate of silver deposition is reduced by additives present in solution 2. The same -0.40 V overpotential is seen for scan 1 at the patterned nickel nanoband (Fig. 2e), but a large overpotential of $-(0.30-0.35)$ V persists for scans 2 and 3 – in contrast to the behavior seen for the nanoband in solution 1. Thus, the proprietary additives present in solution 2 are effective in suppressing the rate of silver deposition at LPNE patterned electrodes even after an initial voltammetric scan.

Three conclusions based on these observations are the following: (1) The onsets for silver deposition at the LPNE patterned electrode are more negative by ~ -0.10 V relative to the flat nickel electrode for both solutions. One explanation for this shift is the rapid depletion of Ag^+ from the narrow trench present in the LPNE template, coupled with slow Ag^+ transport into this trench from the bulk solution. (2) Overpotentials for silver nucleation are significantly larger in solution 2 as compared with solution 1 at both electrodes. (3) The rate of silver deposition from solution 2 is impeded as compared with solution 1 at both electrodes.

Based on the disparate voltammetric behavior of these two silver plating solutions, two pulse waveforms (Fig. 2c and f) optimized for these two solutions were developed to efficiently nucleate and grow silver nanowires in the LPNE template. For nanowire growth from solution 1 (Fig. 2c), this program involves the application of a nucleation pulse of -0.30 V \times 10 ms followed by growth at -0.070 V for a duration appropriate for the desired wire width (see below). In solution 2 (Fig. 2f), a much more aggressive nucleation pulse of -1.4 V \times 750 ms followed by growth at -0.475 V was employed to compensate for the greater nucleation barrier revealed by the

voltammetry results. The voltage range from $-(0.470-0.475)$ V represented the most positive values for which silver nanowires were obtained. Within this potential range, the dendritic growth of silver was suppressed and the width uniformity of the deposited silver nanowires was optimized. These two deposition programs produced silver nanowires that were remarkably similar, in terms of shape and dimensional uniformity but the microstructure of these nanowires were distinctly different, as documented below.

3.2. Dimensional control

Atomic force microscopy (AFM) images of an array of linear silver nanowires prepared from solution 2 are shown in Fig. 3a and b. AFM images of nanowires prepared from solution 1 were indistinguishable from those shown here. These images reveal that the nickel template and photoresist layers can be cleanly and selectively removed from the surface following silver nanowire growth (steps 6 and 7 of Fig. 1) without damaging the silver nanowires and without releasing these nanowires or altering their position on the glass surface. The thickness uniformity of these nanowires can be assessed by measuring cross-sections using AFM (Fig. 3a–c). The wire height seen in these cross-sections is constant to within 10–15% of the mean height. Moreover, the nanowire total height equals the thickness of the nickel film (Fig. 3d) deposited in the first step of the LPNE process (Fig. 1, step 1).

The width of these silver nanowires is most accurately measured using scanning electron microscopy (SEM). Again, no significant differences between the nanowires obtained from solutions 1 and 2 were observed. Nanowires deposited at $5 \mu\text{m}$ pitch from solution 2 are shown in Fig. 4. The width of these nanowires was adjusted by varying the duration of the growth time. Plots of wire width vs. growth time (Fig. 4e) are approximately linear and virtually

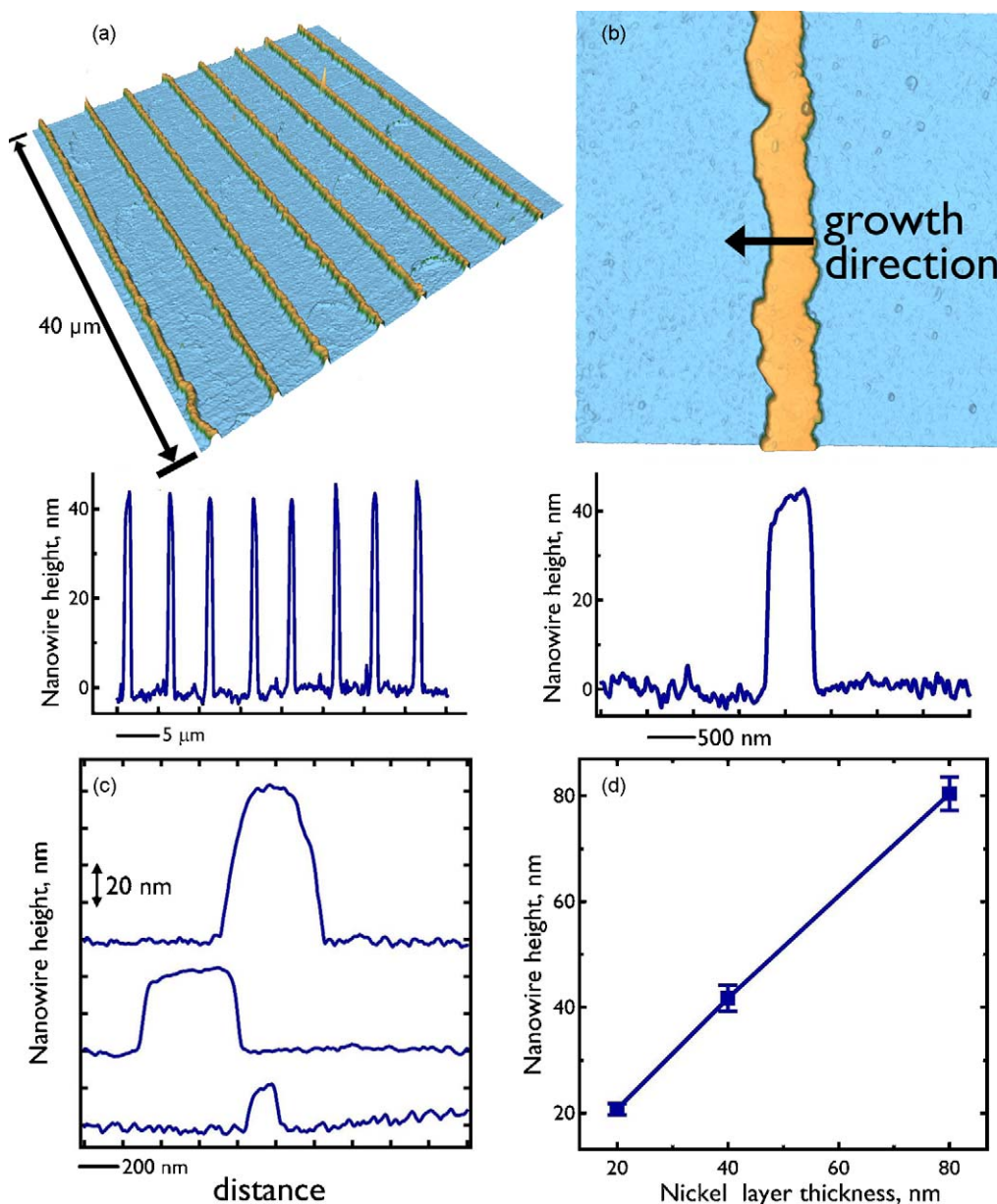


Fig. 3. Atomic force micrographs at low magnification (a, $40\ \mu\text{m} \times 40\ \mu\text{m}$) and higher magnification (b, $5.0\ \mu\text{m} \times 5.0\ \mu\text{m}$) of silver nanowires. The black arrow indicates the growth direction. (c) Amplitude traces of three kinds of silver nanowires prepared using nickel films with the thickness of 20 nm, 40 nm, and 80 nm, respectively. (d) Plot of the mean height for produced silver nanowires reveals the linear dependency of the nickel layer thickness. (For interpretation of the references to color in this figure legend, the reader is referred to the web version of this article.)

identical for these two plating solutions. This result is somewhat surprising since the nucleation pulse of 750 ms used for solution 2 is a factor of 75 longer than that used in solution 1. We speculate that the reason silver nanowires prepared from solution 2 are not wider than those obtained from solution 1 is that both of these nucleation pulses substantially depletes silver from the solution between neighboring nanowires, which are spaced by $5\ \mu\text{m}$. This explanation is supported by the following analysis: the excursion of the diffusion layer from the nickel edge, x , can be approximated as: $x = \sqrt{2Dt}$, where the diffusion coefficient, D , can be approximated at $1 \times 10^{-5}\ \text{cm}^2\ \text{s}^{-1}$ and t is the nucleation pulse duration. For t values of 750 and 10 ms, x is 39 and $4.5\ \mu\text{m}$, respectively. Thus, in both cases the diffusion layer can be expected to encompass the entire interwire distance and silver ion is likely to be depleted from this volume by both of these nucleation pulses. Error bars shown in Fig. 4e document the standard deviation of the wire width and provide an indication of the wire width uniformity which

was somewhat better for nanowires prepared using solution 2. The most important conclusion of these data is that the duration of the growth pulse affords control over the nanowire width over the range from 100 to 400 nm.

3.3. Structural characterization

Grazing incidence X-ray diffraction (GIXRD) provides a powerful method for the characterization of the nanowires produced using LPNE that does not require the removal of nanowires from the glass surface. Samples suitable for GIXRD measurements were prepared by patterning linear silver nanowires at high number density – typically with an interwire spacing of 2–5 μm . An optical micrograph of a silver nanowire array suitable for this purpose (Fig. 5a) shows hundreds of linear silver nanowires. GIXRD patterns were acquired by fixing the incident angle for X-rays, collimated using parallel beam optics, at a value below the critical angle and translating

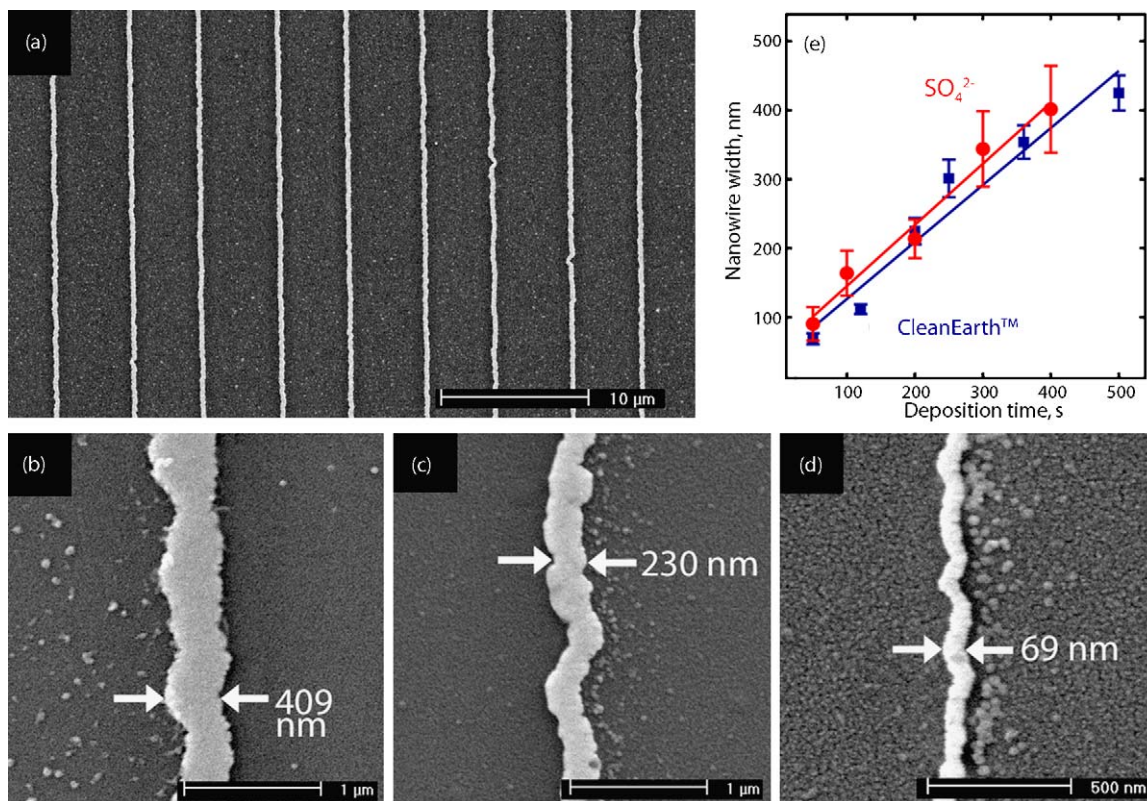


Fig. 4. Scanning electron microscopy (SEM) images of (a) a silver nanowire array at a 5 μm lateral pitch. (b) Different widths of silver nanowires by different deposition time. (c) The quasi-linear correlation can be observed between the mean widths of the generated nanowires and the corresponding deposition time from a sulfate-based aqueous bath (red) and the commercial silver plating solution (blue). (d) The energy-dispersive X-ray (EDX) analysis confirms the composition of the silver nanowire. (For interpretation of the references to color in this figure legend, the reader is referred to the web version of this article.)

the analyzer through an arc of 2θ to record the diffraction pattern (Fig. 5b) [23]. GIXRD patterns (Fig. 5c) for the two plating solutions both show five reflections assignable to fcc silver as indicated. The intensities seen for both experimental patterns track the intensities expected from the model pattern (Fig. 5c, bottom) indicating that silver grains are isotropically oriented with respect to the scattering direction [15]. A difference in the diffraction line widths, however, is observed with nanowire deposited from solution 1 producing narrower diffraction lines than those obtained from solution 2. If it can be assumed that X-ray line broadening is dominated by the crystallite diameter as opposed to lattice strain, the

average crystallite size can be estimated from the Debye–Scherrer equation [28]:

$$d = \frac{0.9\lambda}{\beta \cdot \cos \theta}$$

where d is the mean crystallite diameter, λ is the X-ray wavelength, β is the full width of the diffraction line at half its maximum intensity, and θ is the diffraction angle. Silver nanowires deposited from solution 1 have a mean grain diameter of ~24 nm whereas those deposited from solution 2 have a mean grain diameter of ~15 nm. It is important to note that the scattering vector for the

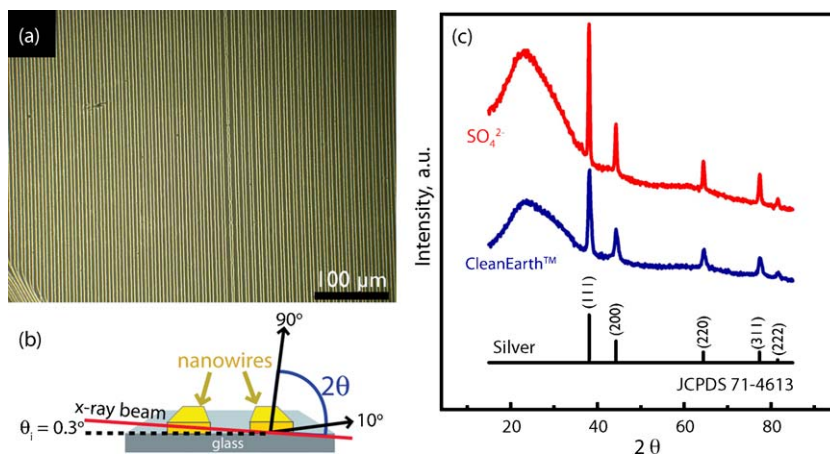


Fig. 5. (a) Optical micrograph of an array of silver nanowires prepared using LPNE and used for the acquisition of grazing incidence X-ray diffraction (GIXRD). The distance between nanowires in this array was $\approx 5 \mu\text{m}$ pitch. (b) Schematic diagram showing the geometry of the GIXRD experiment involving a fixed 0.3° angle of incidence, θ_i . (c) GIXRD patterns for nanowire deposited using solution 1 (labeled SO₄²⁻) and solution 2 (labeled Clean Earth™). The assignment of reflections to fcc silver (JCPDS 71-4613) is shown at bottom. A broad reflection at 25° is produced by diffuse scattering from the glass surface.

GIXRD measurement is not fixed along the surface normal, as it is in the conventional Bragg–Brentano geometry, but it nevertheless has its principle component perpendicular to the surface so to a first approximation, it is the grain dimension perpendicular to the surface that is obtained using this measurement.

As compared with GIXRD, transmission electron microscopy (TEM) provides complimentary information relating to the grain structure of these nanowires both because it is a real-space imaging technique and because it is the in-plane, not out-of-plane, grain dimensions that are seen. TEM images of nanowires obtained from solution 1 (left) and solution 2 (right) are compared in Fig. 6a. Dark lines in these images are associated with grain boundaries. For either of these nanowires, if an individual grain is examined at high magnification lattice-fringes are observed (e.g., Fig. 6b). Here

the distance between adjacent lattice planes is $\sim 2.40 \text{ \AA}$, close to that expected for the d -spacing along the (1 1 1) plane of silver (2.36 \AA , JCPDS 71-4613). Selected-area electron diffraction analysis (Fig. 6c), acquired from a $10 \mu\text{m}$ diameter area of the surface encompassing several nanowires deposited from solution 2, shows concentric rings of diffracted electron intensity as expected for polycrystalline materials.

A histogram of crystallite diameters can be constructed by acquiring TEM images of the same nanowire section at a series of tilt angles relative to the electron beam axis. In each of these images, a unique subset of the grains meets the condition for diffraction of the electron beam and these grains appear black in the transmission image [29], enabling the accurate measurement of grain dimensions. These histograms (Fig. 6d) reveal a significant differ-

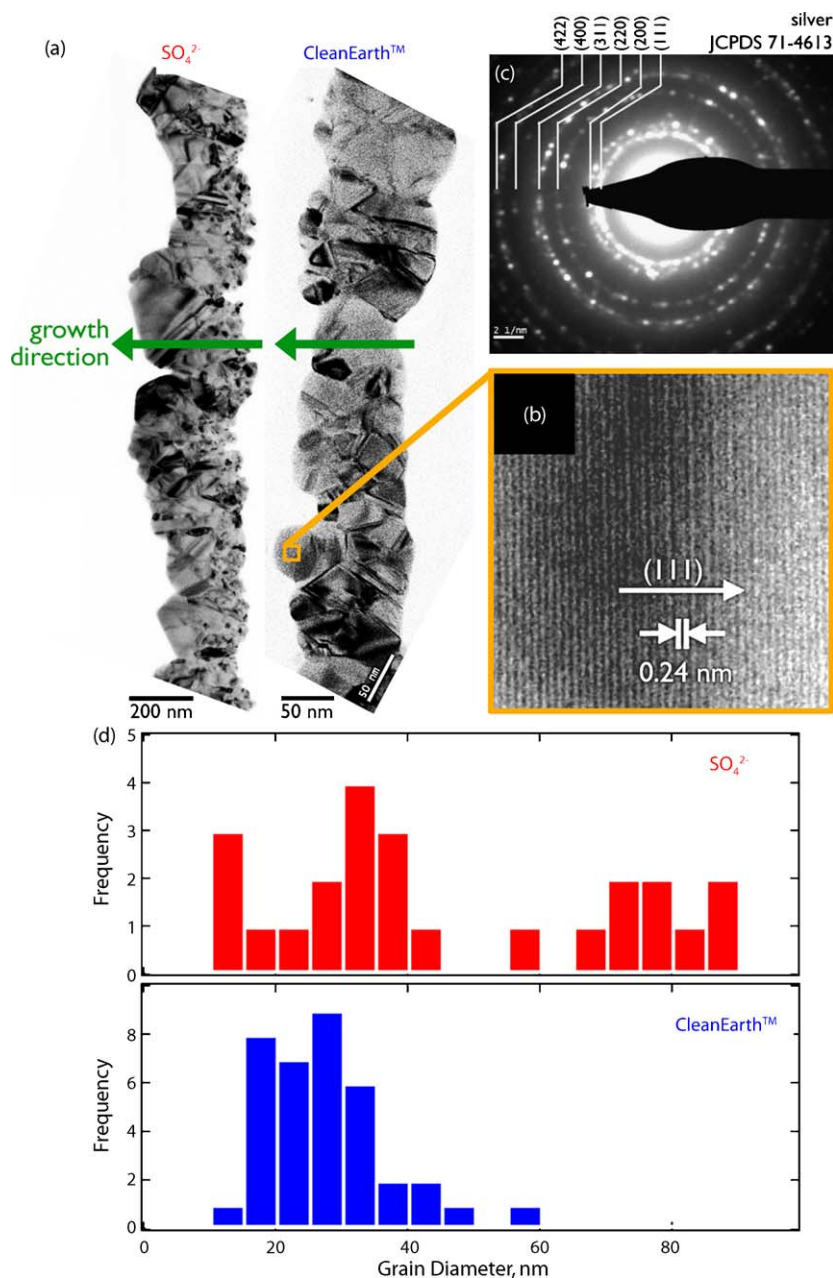


Fig. 6. (a) Transmission electron micrographs (TEM) of two silver nanowires, both 20 nm in thickness. The wire at left was obtained from solution 1 and the wire at right from solution 2. (b) high magnification TEM image showing closest packed silver atomic layers along (1 1 1) within a single crystalline grain. This lattice resolved image reveals the interplane distance of 2.40 \AA consistent with fcc silver. (c) Selected-area electron diffraction (SAED) pattern for the nanowire prepared from solution 2. The pattern seen for the wire deposited from solution 1 was virtually identical. Concentric rings, characteristic of polycrystallinity, are assigned to the reflections of fcc silver (JCPDS 71-4613). (d) Histograms of the crystallite size for silver nanowires prepared from the two plating solutions, determined by tilt-resolved TEM image sequences.

ence between nanowires deposited from solution 1 and solution 2. Specifically, nanowires deposited from solution 1 show a bimodal grain diameter distribution with mean values near 30 and 80 nm. This bimodal microstructure is already apparent from the TEM image shown in Fig. 6a (left) where it can be clearly seen that the grain size increases dramatically with distance away from the nickel edge (from right to left in Fig. 6a). The largest grains seen along the left edge of that nanowire are in the 70–100 nm range whereas the smaller grains at the right edge are 10–40 nm in size. The increase in grain diameter during nanowire growth from solution 1 could be the result of saccharine depletion since saccharine is a nucleation promoter in this system. In contrast, nanowires obtained from solution 2 (e.g., Fig. 6a, right) are composed entirely of 10–40 nm crystallites. It is important to note here that we found it impossible to produce continuous silver nanowires using solution 1 with the omission of saccharine so it plays an essential role. Further investigations will be required to fully understand the mechanism by which saccharine promotes continuous nanowire growth. This result, together with the less profound grain size differences exposed by GIXRD, suggests that additives present in the commercial plating solution (solution 2) are more effective than saccharine (present in solution 1) at promoting the formation of new silver nuclei at the relatively positive potentials used to propagate silver nanowire growth (Fig. 2c and f). The silver grain diameter seen at the nickel edge can be used to estimate the minimum nanowire width obtainable using this process and this minimum width is in the 10–40 nm range, similar to the smallest gold and platinum nanowires obtained using the LPNE process [21,23,25].

4. Conclusion

The LPNE method outlined in this paper provides a robust method for the fabrication of ultra-long, polycrystalline silver nanowires. The following are the key conclusions pertaining to this process:

1. The LPNE process used for the fabrication of gold, platinum, and palladium nanowires, involving a sacrificial nickel electrode, can be adapted to the growth of silver nanowires using either of two silver plating solutions.
2. Compared with the preparation by LPNE of gold, platinum and palladium nanowires, we encountered greater difficulty obtaining continuous nanowires of uniform width.
3. This issue was addressed by employing a nucleation pulse at the beginning of the deposition process to promote silver nucleation. The parameters for the nucleation pulses were optimized for the two plating solutions employed here.
4. Control of the silver nanowire height is not affected by either of these complications; as with other metals, the wire height is controlled by the thickness of the evaporated nickel film over the range from 20 to 80 nm.
5. The silver nanowires obtained from these two solutions are indistinguishable externally, but they have distinctly different grain structures. The nanowires obtained from solution 1 show an increase in grain diameter from a mean value near 30 nm

near the nickel edge to values near 80 nm at the other edge of the nanowire, just 200 nm distant from the nickel edge. No evolution in grain diameter with growth time was observed for the nanowires obtained from solution 2 where a mean value near 30 nm applied across the diameter of the nanowire.

Acknowledgements

The authors gratefully acknowledge the financial support by the National Science Foundation (CHE-0956524) and the *School of Physical Sciences, Center for Solar Energy* at UCI. Electron microscopy was performed at the Materials Characterization Center, LEXI/CALIT2, of the University of California-Irvine. The constructive comments of a reviewer of this paper are also gratefully acknowledged.

References

- [1] M.V. Sosnova, N.L. Dmitruk, A.V. Korovin, S.V. Mamykin, V.I. Mynko, O.S. Lytvyn, *Applied Physics B: Lasers and Optics* (2009).
- [2] H. van der Lem, A. Moroz, *Journal of Optics A: Pure and Applied Optics* 2 (2000) 395.
- [3] H. Dittbacher, A. Hohenau, D. Wagner, U. Kreibitz, M. Rogers, F. Hofer, F.R. Aussenegg, J.R. Krenn, *Physical Review Letters* 95 (2005) 4.
- [4] A.L. Pyayt, B. Wiley, Y. Xia, A. Chen, L. Dalton, *Nature Nanotechnology* 3 (2008) 660.
- [5] G. Schider, J.R. Krenn, A. Hohenau, H. Dittbacher, A. Leitner, F.R. Aussenegg, W.L. Schaich, I. Puscasu, B. Monacelli, G. Boreman, *Physical Review B* 68 (2003) 4.
- [6] M. Moskovits, *Reviews of Modern Physics* 57 (1985) 783.
- [7] P. Mohanty, I. Yoon, T. Kang, K. Seo, K.S.K. Varadwaj, W. Choi, Q.H. Park, J.P. Ahn, Y.D. Suh, H. Ihee, B. Kim, *Journal of the American Chemical Society* 129 (2007) 9576.
- [8] C. Zuo, P.W. Jagodzinski, *The Journal of Physical Chemistry B* 109 (2005) 1788.
- [9] C.-W. Kuo, J.-Y. Shiu, K.H. Wei, P. Chen, *Chemistry Letters* 37 (2008) 610.
- [10] N.R. Jana, L. Gearheart, C.J. Murphy, *Chemical Communication* (2001) 617.
- [11] Z. Wang, J. Liu, X. Chen, J. Wan, Y. Qian, *Chemistry – A European Journal* 11 (2005) 160.
- [12] M. Barbic, J.J. Mock, D.R. Smith, S. Schultz, *Journal of Applied Physics* 91 (2002) 9341.
- [13] Q. Zhang, Y. Li, D. Xu, Z. Gu, *Journal of Materials Science Letters* 20 (2001) 925.
- [14] R.-L. Zong, J. Zhou, Q. Li, B. Du, B. Li, M. Fu, X.-W. Qi, L.-T. Li, S. Buddhudu, *Journal of Physical Chemistry B* 108 (2004) 16713.
- [15] G. Riveros, S. Green, A. Cortes, H. Gomez, R.E. Marotti, E.A. Dalchiele, *Nanotechnology* 17 (2006) 561.
- [16] P.R. Evans, R. Kulloock, W.R. Hendren, R. Atkinson, R.J. Pollard, L.M. Eng, *Advanced Functional Materials* 18 (2008) 1075.
- [17] E.C. Walter, B.J. Murray, F. Favier, G. Kaltenpoth, M. Grunze, R.M. Penner, *Journal of Physical Chemistry B* 106 (2002) 11407.
- [18] E.C. Walter, M.P. Zach, F. Favier, B.J. Murray, K. Inazu, J.C. Hemminger, R.M. Penner, *ChemPhysChem* 4 (2003) 131.
- [19] B.J. Murray, E.C. Walter, R.M. Penner, *Nano Letters* 4 (2004) 665.
- [20] B.J. Murray, J.T. Newberg, E.C. Walter, Q. Li, J.C. Hemminger, R.M. Penner, *Analytical Chemistry* 77 (2005) 5205.
- [21] E.J. Menke, M.A. Thompson, C. Xiang, L.C. Yang, R.M. Penner, *Nature Materials* 5 (2006) 914.
- [22] Y. Yang, S.C. Kung, D.K. Taggart, C. Xiang, F. Yang, M.A. Brown, A.G. Guell, T.J. Kruse, J.C. Hemminger, R.M. Penner, *Nano Letters* 8 (2008) 2447.
- [23] C. Xiang, S.C. Kung, D.K. Taggart, F. Yang, M.A. Thompson, A.G. Guell, Y. Yang, R.M. Penner, *ACS Nano* 2 (2008) 1939.
- [24] F. Yang, D.K. Taggart, R.M. Penner, *Fast, Nano Letters* 9 (2009) 2177.
- [25] C. Xiang, Y. Yang, R.M. Penner, *Chemical Communication* (2009) 859.
- [26] C. Xiang, A.G. Guell, M.A. Brown, J.Y. Kim, J.C. Hemminger, R.M. Penner, *Nano Letters* 8 (2008) 3017.
- [27] C. Xiang, J.Y. Kim, R.M. Penner, *Nano Letters* 9 (2009) 2133.
- [28] A.L. Patterson, *Physical Review* 56 (1939) 978.
- [29] D.T. Carpenter, J.M. Rickman, K. Barmak, *Journal of Applied Physics* 84 (1998) 5843.